JOURNAL OF CHEMICAL & ENGINEERING DATA

ARTICLE

pubs.acs.org/jced

Phase Behavior of Athabasca Bitumen

Ala Bazyleva,[†] Michal Fulem,[‡,§] Mildred Becerra,[†] Bei Zhao,[†,∥] and John M. Shaw*[,†]

[†]Department of Chemical and Materials Engineering, University of Alberta, Edmonton, Alberta T6G 2G6, Canada

[‡]Department of Physical Chemistry, Institute of Chemical Technology, Prague, Technická 5, CZ-166 28 Prague 6, Czech Republic

[§]Institute of Physics, Academy of Sciences of the Czech Republic, v.v.i., Cukrovarnická 10, CZ-162 53 Prague 6, Czech Republic

[∥]CANMETEnergy, Natural Resources Canada, Devon, Canada, T9G 1A8

Supporting Information

ABSTRACT: The phase behavior of Athabasca bitumen (Alberta, Canada) was determined from nanofiltered permeates and retentates with pentane-asphaltene mass fractions w_A ranging from 0.053 to 0.57, and chemically separated Athabasca pentane maltenes and pentane asphaltenes based on differential scanning calorimetry and rheology measurements from (190 to 570) K at atmospheric pressure. Samples were subject to two sequential heating cycles. Composition, apparent heat-capacity, and phase-angle data were collected and interpreted jointly to define phase diagrams for nanofiltered maltene + nanofiltered asphaltene pseudobinary mixtures for each heating cycle. These pseudocomponents are shown to behave independently. During the first heating cycle, observed phase transitions for maltenes include: a broad low-temperature glass transition with a T_g from (215 to 230) K and a small first-order phase transition with a peak temperature T_{trs} between (320 and 340) K linked to a fraction of Athabasca maltenes undergoing a crystal to liquid transition. These transitions were found in both chemically separated and nanofiltered maltenes. Nanofiltered asphaltenes undergo a two-stage transition from solid to liquid between (260 and 470) K, with the second stage being a glass type transition. The nature of the first stage requires additional study. By contrast, chemically separated pentane asphaltenes undergo a complex transformation from (310 to 530) K comprising overlapping processes including endothermic transitions from solid-to-liquid and solid-to-liquid crystals and an exothermic dissolution of the liquid crystals [Bagheri, S. R., et al. *Energy Fuels* **2010**, *24*, 4327−4332]. Athabasca bitumen comprises a minimum of four phases drawn from liquid, crystalline maltene + glass and/or crystal, and liquid asphaltenes from (260 to 360) K. The phase transition reversibility is discussed, and the phase diagram for Athabasca bitumen is compared with that of Maya crude oil, reported previously [Fulem, M., et al. *Fluid Phase Equilib.* **2008**, *272*, 32−41]. Multiphase behavior appears to be a general phenomenon, but phase diagram details appear to vary from feedstock to feedstock.

1. INTRODUCTION

Athabasca bitumen (Canada) is a hydrocarbon energy resource of global significance.[1,2] The exploitation of Athabasca bitumen whether by surface mining or by in situ methods is a multistage process[3] complicated by extreme and variable atmospheric conditions. Accurate thermophysical and transport property data are required for the development and optimization of production, transportation, and refining processes for this hydrocarbon resource. Since Athabasca bitumen is a complex fluid, phase-equilibrium data and phase behavior reversibility knowledge are crucial for all stages of process design and operation and for process design software development.

The opacity of bitumen to visible light and the length scales of phase domains[4] preclude the study of phase behavior by conventional methods. A protocol based on a combination of nanofiltration for sample preparation, calorimetry, rheometry, and a predictive correlation for solid-state heat capacity is employed. The protocol, illustrated previously for the creation of a phase diagram for Maya crude oil,[5] provides: (1) thermodynamic parameters of phase transitions (temperatures or temperature ranges, enthalpies, etc.); (2) state and number of phases at fixed temperatures; (3) information on the reversibility of phase transformations; in addition to (4) the phase diagram. Information related to phase behavior reversibility is extremely important because there are several heating−cooling cycles arising in bitumen production and pipelining processes, which can affect thermophysical and transport properties of bitumen without composition change.

In the present work, the Athabasca bitumen phase diagram is presented as a pseudobinary diagram based on samples partitioned by nanofiltration. From our prior work,[6] nanofiltration partitions feed stocks into maltene-enriched permeate samples and asphaltenes-enriched retentate samples, without the use of solvents. The properties of these samples are also compared with those of chemically separated pentane maltenes and pentane asphaltenes.

2. EXPERIMENTAL SECTION

2.1. Materials. Athabasca bitumen (Alberta, Canada) was obtained from Syncrude Canada Ltd. The sample was characterized as a coker feed. It is derived from mined bitumen subjected to warm-water extraction, naphtha dilution, and naphtha recovery by distillation between (523 and 623) K. Some volatile constituents present initially were lost during sample preparation. Samples with differing

Received: April 10, 2011
Accepted: May 31, 2011
Published: June 28, 2011

Table 1. Composition (in Mass Fraction) of Athabasca Bitumen Related Samples[a]

component	AB C_5 maltenes	P10	P20	P50	Athabasca bitumen	R200	R10	AB C_5 asphaltenes
				SARA Analysis[b]				
saturates	0.178 ± 0.021	0.189 ± 0.021 (0.20)[c]	0.184 ± 0.021 (0.201)[c]	0.171 ± 0.021 (0.20)[c]	0.161 ± 0.021 (0.20)[c]	0.094 ± 0.021 (0.19)[c]	0.089 ± 0.021 (0.21)[c]	0
aromatics	0.553 ± 0.023	0.567 ± 0.023 (0.60)[c]	0.530 ± 0.023 (0.59)[c]	0.534 ± 0.023 (0.62)[c]	0.485 ± 0.023 (0.60)[c]	0.260 ± 0.023 (0.52)[c]	0.254 ± 0.023 (0.59)[c]	0
resins	0.269 ± 0.012	0.191 ± 0.012 (0.20)[c]	0.182 ± 0.012 (0.20)[c]	0.159 ± 0.012 (0.18)[c]	0.168 ± 0.012 (0.21)[c]	0.146 ± 0.012 (0.29)[c]	0.087 ± 0.012 (0.20)[c]	0
C_5 asphaltenes	0	0.053 ± 0.001	0.104 ± 0.006	0.136 ± 0.010	0.186 ± 0.018	0.50 ± 0.13	0.57 ± 0.17	1
				Elemental Analysis[d]				
C	0.837 ± 0.010	0.842 ± 0.010	0.843 ± 0.010	0.838 ± 0.010	0.832 ± 0.009	0.811 ± 0.009	0.812 ± 0.009	0.771 ± 0.009
H	0.109 ± 0.004	0.105 ± 0.004	0.100 ± 0.004	0.106 ± 0.004	0.097 ± 0.004	0.088 ± 0.003	0.091 ± 0.004	0.074 ± 0.003
N	0.003 ± 0.002	0.003 ± 0.002	0.004 ± 0.002	0.004 ± 0.002	0.004 ± 0.002	0.007 ± 0.002	0.007 ± 0.002	0.012 ± 0.002
S	0.044 ± 0.002	0.050 ± 0.002	0.050 ± 0.002	0.052 ± 0.002	0.053 ± 0.002	0.061 ± 0.002	0.067 ± 0.002	0.081 ± 0.002
O	0.003 ± 0.001	0.005 ± 0.001	0.017 ± 0.003	0.009 ± 0.001	0.017 ± 0.003	0.022 ± 0.003	0.013 ± 0.002	0.010 ± 0.002

[a] "P" and "R" stand for permeates and retentates, respectively; for example, "P10" stands for the permeate obtained by nanofiltration through a membrane with the 10 nm pore size (see ref 6 for details). [b] The SARA analysis errors are given as repeatability according to the ASTM. The SARA analysis is not well-defined for samples with more than 0.35 mass fraction of asphaltenes. [c] Composition on an asphaltene-free basis. [d] The elemental analysis errors are given as repeatability according to the ASTM.

asphaltene content were prepared by solvent-free nanofiltration using 10 nm, 20 nm, 50 nm, and 200 nm filters at 473 K. A detailed description of the nanofiltration apparatus and the experimental procedure is presented elsewhere.[6] Abbreviations "P" and "R" refer to permeate and retentate, respectively. Chemically separated asphaltene and maltene samples were prepared by precipitation with pentane according to the following procedure. Athabasca bitumen (AB) pentane (C_5) asphaltenes were precipitated at room temperature and atmospheric pressure by addition of pentane to bitumen at a 40:1 volume ratio. The mixture was stirred overnight at room temperature and then filtered in two steps by vacuum filtration using a Fisher brand filter paper Q2 with a pore size between (1 and 5) μm and then using a 0.22 μm Millipore membrane comprising mixed cellulose esters. The filtration membranes and the flask were washed with small volumes of pentane to eliminate residual oil until the filtrate became colorless. The membranes with precipitated material (pentane asphaltenes) were dried at 373 K for 30 min and afterward placed overnight in a vacuum oven operated at 9 kPa. Permeate samples were distilled at 313 K to remove pentane to produce pentane maltenes.

SARA analyses (Table 1) for Athabasca bitumen, permeate and retentate samples, and chemically separated maltenes and asphaltanes were carried out according to ASTM D2007 for saturates, aromatics, and resins and ASTM D3279 for pentane (C_5) asphaltenes. Elemental analyses are also reported in Table 1. Carbon, hydrogen, and nitrogen were determined using ASTM D5291 on a LECO CHN-1000 analyzer. Sulfur was determined using ASTM D1552 on a LECO SC-432 sulfur analyzer, and oxygen was determined using a PE 2400 Series II analyzer according to refs 7 and 8. All analyses were performed at the National Centre for Upgrading Technology (NCUT), Devon, Canada. For detailed information concerning the applicable concentration ranges, analysis methods precision, repeatability and reproducibility, and additional elemental analyses readers are referred elsewhere.[6]

2.2. Calorimetric Measurements. Apparent heat capacities were measured in the temperature range (190 to 570) K using a differential scanning calorimeter TG-DSC 111 (Setaram, France). The DSC calorimeter was calibrated in accordance with the recommendations developed by the GEFTA working group "Calibration of Scanning Calorimeters".[9−13] A heating-rate dependent temperature calibration to ITS-90 was performed using indium, tin, lead, zinc (for all, mass fractions were 0.99999, Sigma-Aldrich Co.), naphthalene (mass fraction 0.997, Sigma-Aldrich Co.), and gallium (mass fraction 0.999995, Sigma-Aldrich Co.), as recommended by GEFTA,[9−13] as well as using cyclohexane (mass fraction 0.9999, Sigma-Aldrich Co.), a primary reference according to ref 14. To cover the temperature range down to 200 K, two additional compounds with well-defined triple points were chosen for the temperature calibration: octane (mass fraction 0.998 determined by GC, Fluka/Sigma-Aldrich Co.; T_{fus} = 216.42 K[15,16]) and decane (mass fraction 0.9999 determined by GC, Fluka/Sigma-Aldrich Co.; T_{fus} = 243.54 K[15,16]). Energy calibration was performed using the Joule effect method in the factory and checked by measuring the enthalpies of fusion, $\Delta_{fus}H_m$, of galium, naphthalene, indium, and tin. The agreement with recommended literature values[9−14,17] was within 1 %. The measured enthalpies of fusion for octane and decane agreed with the literature values[15,16] within 2 %. The heat capacity c_p calibration was performed using naphthalene, a secondary reference material for c_p measurements recommended by ICTAC,[14] and synthetic sapphire, a primary reference material according to NIST (SRM 720) and ICTAC.[14] The uncertainty of the c_p measurements was estimated to be: less than 10 % in the temperature interval from (190 to 220) K, less than 6 % from (220 to 240) K, about 3 % between (240 and 280) K, and less than 2 % in the temperature range from (290 to 570) K. Because of irreproducible device artifacts, the range from (280 to 290) K was not used.

Heat capacity measurements were performed in three stages:

(1) Samples were cooled to 173 K at a cooling rate of 0.083 $K \cdot s^{-1}$ using a liquid nitrogen pump, then heated from (173 to 313) K at a heating rate of 0.083 $K \cdot s^{-1}$. Heat-flow stabilization was achieved at (190 to 200) K, but large artifacts were observed above 280 K.

(2) Samples were cooled to 258 K at a cooling rate of 0.083 $K \cdot s^{-1}$ using a liquid nitrogen pump, then heated from (258 to 353) K at a heating rate of 0.083 $K \cdot s^{-1}$. No artifacts were observed, but heat-flow stabilization was achieved at (285 to 290) K.

(3) Samples were heated from (293 to 573) K at a heating rate of 0.083 $K \cdot s^{-1}$. Heat-flow stabilization was achieved at (305 to 310) K.

The heat-capacity data from these three stages were treated jointly to obtain self-consistent temperature dependences for

heat capacity from (190 to 280) K and from (290 to 570) K. All heat capacity data were obtained using a continuous three-step method[18] —(1) empty, (2) reference material (sapphire), and (3) sample under study—in a measuring cell; a reference cell was empty in all three runs. The measurements were carried out with isothermal periods of 3600 s (or 1800 s when starting below 290 K) at the beginning and the end of each trial. The typical mass of organic samples was (60 to 50) mg (with uncertainty of 0.05 mg). Hermetically sealed stainless-steel cells, with a maximum pressure of 10 MPa at 573 K, were used for all experiments. The tightness of seals was checked by measuring sample + cell mass before and after experiments. Mass loss was not detected in any of the experiments. Consequently, sample vaporization did not contribute significantly to heat-flow measurements.

2.3. Rheological Measurements. Rheological experiments were carried out in the oscillatory mode using a controlled stress/strain Bohlin Gemini HR Nano rheometer (Malvern Instruments Limited, UK). The following measuring configurations were used:

(1) Parallel plates (25 mm diameter) with a Peltier assembly using the principle of the Peltier heat pump, allowing measurements from (243 to 453) K with temperature stability of ± 0.2 K. This configuration was used for all samples, except for AB C_5 maltenes and C_5 asphaltenes.

(2) Parallel plates (25 mm diameter) with an extended temperature cell (ETC) using a forced gas system to heat and cool the sample. The ETC can also be fitted with a low temperature extension (LTE)—cooling with liquid nitrogen (vapor)—for measurements below ambient temperature. The ETC in these two complementary configurations (with and without LTE) covers the temperature range from (123 to 823) K with a stability better than ± 0.2 K. This configuration was used for AB C_5 maltenes and asphaltenes and to extend the temperature ranges of measurements for other samples.

Sample temperatures were measured with thermocouples (calibrated to ITS-90 using a PT100 resistance thermometer) inserted into the middle of the lower plate (ETC) or in the lower base (Peltier assembly). All experiments were conducted under nitrogen atmosphere to avoid sample oxidation. The gap between the parallel plates was (650 and 1000) μm depending on the range of viscosity values studied. The temperature sweep measurements were performed with the cooling and heating rates of 0.050 $K \cdot s^{-1}$ at a constant frequency of 1 Hz. Constant shear stress or constant shear strain were applied for all samples. Complex viscosity, shear moduli, and phase angles were recorded.

The experimental conditions and the operating parameter values for the rheological measurements were validated using certified viscosity standards N2700000SP, N74B, N1400B, and N115B (from CANNON Instrument Company, USA), and standard oils #12 and U3600 (from the Paint Research Association, UK). The agreement with the recommended data in the certified temperature range (244 to 349) K was within 5 % for the parallel-plate Peltier assembly and for the parallel plates in the ETC without cooling, and within 10 % for the parallel plates in the ETC with liquid nitrogen cooling (LTE). These values are assumed to be uncertainties of the viscosity measurements.

3. HEAT CAPACITY CORRELATION FOR ORGANIC SOLIDS

For materials as complex as bitumen, phase transitions arise over broad temperature intervals. The starting points and end points for solid-to-liquid transitions and the enthalpy of transitions can be difficult to detect. An accurate and reliable baseline is essential. For this purpose, we use a predictive correlation for the specific heat capacity of crystalline organic solids:[19−21]

$$c_p^{(s),\mathrm{pred}}/(\mathrm{J \cdot K^{-1} \cdot g^{-1}}) = 3R(A_1\alpha + A_2\alpha^2)\left(\frac{\theta}{T}\right)^2 \frac{\exp(\theta/T)}{[\exp(\theta/T)-1]^2} + (C_1\alpha + C_2\alpha^2)T + (D_1\alpha + D_2\alpha^2)T^2 \quad (1)$$

where $c_p^{(s),\mathrm{pred}}$ is the specific solid-state heat capacity, T is temperature (in K), $A_1 = 1.3183 \cdot 10^{-2}$, $A_2 = 2.4938 \cdot 10^{-1}$, $C_1 = 2.6526 \cdot 10^{-2}$, $C_2 = -2.4942 \cdot 10^{-2}$, $D_1 = 2.5000 \cdot 10^{-5}$, $D_2 = -1.2300 \cdot 10^{-4}$, and θ = 151.8675 K are the universal parameters. The parameter α, proportional to the number of atoms per unit mass, is evaluated from elemental composition:

$$\alpha = \sum_{i=1}^{n} w_i/M_i \quad (2)$$

where n is the number of element types in the sample, M_i is the molar mass of element i in $\mathrm{g \cdot mol^{-1}}$, and w_i is the mass fraction of element i in the sample.

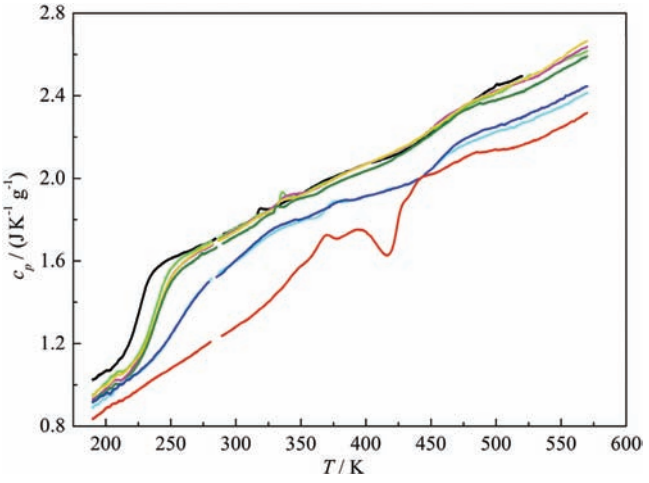

Figure 1. Experimental specific heat capacity values for heating cycle 1: black line, C_5 maltenes with $w_A = 0$; light green line, P10 with $w_A = 0.053$; pink line, P20 with $w_A = 0.104$; yellow line, P50 with $w_A = 0.136$; dark green line, AB bitumen with $w_A = 0.186$; cyan line, R200 with $w_A = 0.50$; blue line, R10 with $w_A = 0.57$; red line, C_5 asphaltenes with $w_A = 1$.

4. RESULTS

Apparent specific heat capacity data as well as values calculated from eqs 1 and 2 using the elemental compositions from Table 1 are provided as Supporting Information (File 1 − Heat Capacity Data). Two successive heating cycles up to 573 K were carried out for each sample. In addition, sample R200 was subjected to three successive heating cycles up to 573 K as a further check on the reversibility of the apparent heat capacity values. The specific heat capacities for the first heating cycle are shown in Figure 1. The samples exhibit several phase transitions. The first transition, with a shape typical of glass-type transitions, starts at temperatures between (210 and 240) K for all samples, except for C_5 asphaltenes. A second transition, with a shape typical of a first-order transition, is observed between (310 and 360) K for maltene-rich samples. A third and more complex set of transitions is detected for the AB C_5 asphaltenes

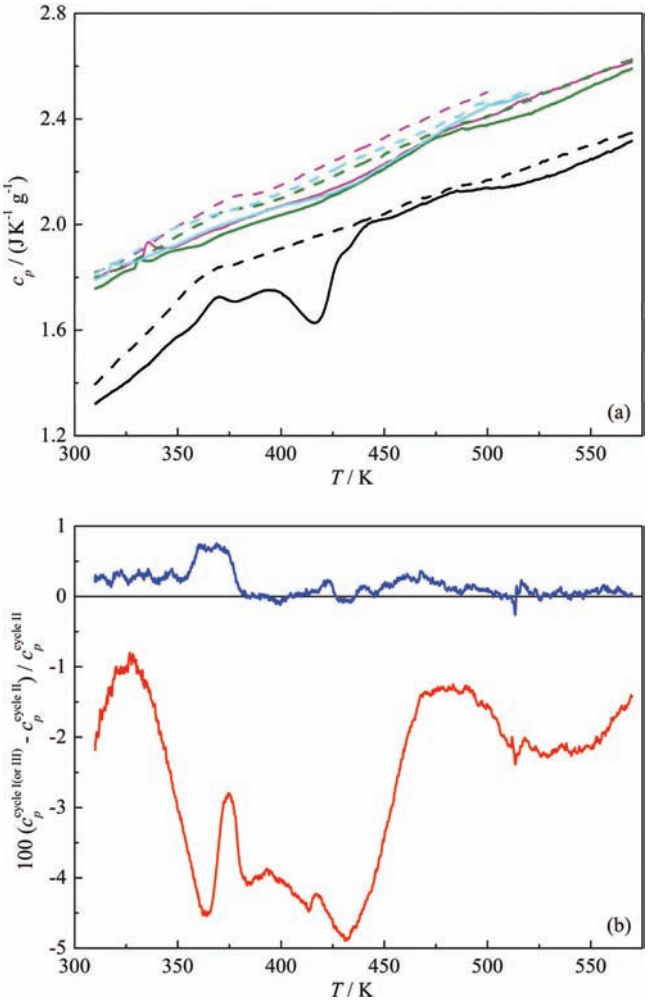

Figure 2. (a) Comparison between the first heating cycle (solid line) and second heating cycle (dashed line) specific heat capacity values for: C_5 maltenes (cyan); sample P10 (pink); AB bitumen (dark green); C_5 asphaltenes (black). (b) Deviation of the specific heat capacities for sample R200 measured during heating cycle 1 (red line) and heating cycle 3 (blue line) from values obtained during heating cycle 2.

from (310 to 530) K. The apparent heat capacities for the second heating cycle differ markedly from the first heating cycle as illustrated in Figure 2a for selected samples. The specific heat capacities are consistently higher for all samples during the second heating cycle and the transition between (310 and 360) K is absent. The complex phase transition from (310 to 530) K for C_5 asphaltenes is replaced with a glass type-transition. For subsequent heating cycles there is no further change as illustrated in Figure 2b for sample R200 where differences in c_p values obtained during the second and third heating cycles fall within the uncertainty of the measurements.

For the c_p measurements in Figure 1, samples were cooled from room temperature at 0.083 K·s^{-1}. To study more deeply the nature of the low-temperature glass-type phase transition, two cooling schemes with reduced cooling rates were carried out for the least viscous sample, C_5 maltenes. The heating rate for the heat capacity measurements was kept fixed at 0.083 K·s^{-1}. The results are presented in Figure 3 and Supporting Information (File 1, Heat Capacity Data).

Rheological measurements are reported in detail in the Supporting Information (File 2, Rheological Data). Phase angle

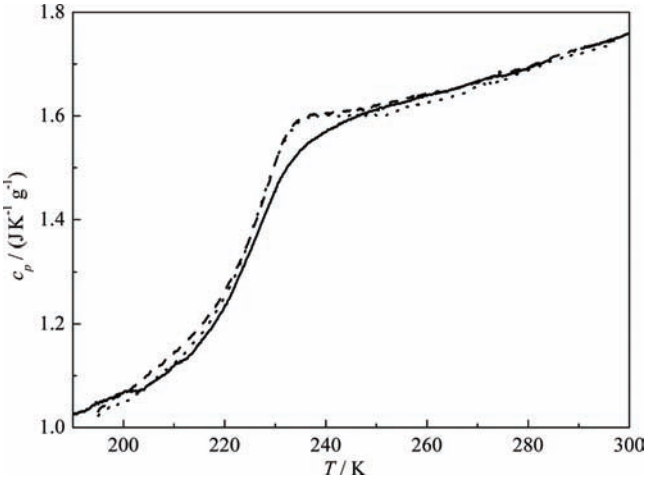

Figure 3. Impact of cooling rate on the apparent heat capacity of AB C_5 maltenes near its glass transition: solid line, cooling rate of 0.083 K·s^{-1}; dashed line, cooling rate of 0.017 K·s^{-1}; dotted line, complex cooling procedure: from (313 to 233) K cooling rate of 0.017 K·s^{-1}, then 1800 s of annealing at 233 K, from (233 to 223) K cooling rate of 0.017 K·s^{-1}, then 1800 s annealing at 223 K, from (223 to 173) K cooling rate of 0.017 K·s^{-1}.

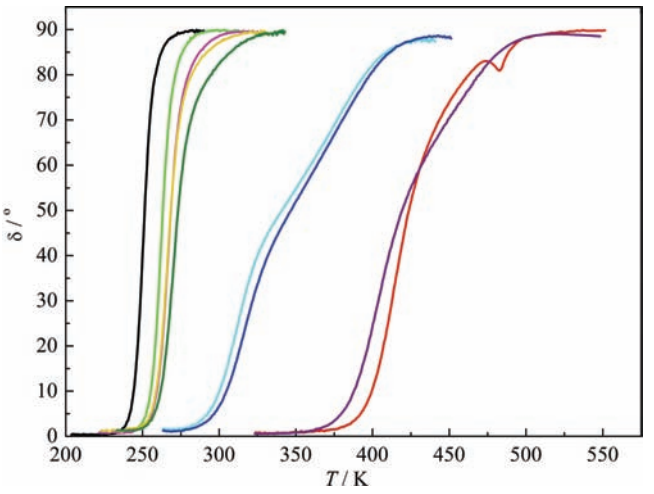

Figure 4. Phase angle (δ) values for: black line, C_5 maltenes with $w_A = 0$; light green line, P10 with $w_A = 0.053$; pink line, P20 with $w_A = 0.104$; yellow line, P50 with $w_A = 0.136$; dark green line, AB bitumen with $w_A = 0.186$; cyan line, R200 with $w_A = 0.50$; blue line, R10 with $w_A = 0.57$; C_5 asphaltenes with $w_A = 1$ (red line, heating cycle 1; purple line, heating cycle 2).

data are presented in Figure 4. All samples reveal a continuous transformation from a solid-like (phase angle of 0°) to a liquid-like state (phase angle of 90°). The phase-angle change with temperature was reproducible over the time scale of the measurements, except for C_5 asphaltenes. Results for both the first and second heating cycles for C_5 asphaltenes are reported in Figure 4.

To enrich our understanding of glass transitions in the current context, DSC and rheology measurements were performed with polybutene, a glass-forming polymer. Heat capacity and phase angle data for polybutene (CAS RN 9003-29-6, a random copolymer of 2-methylprop-1-ene and but-1-ene, and available as Cannon certified viscosity standard N2700000SP) are listed in Supplementary Data (File 1, Heat Capacity Data and File 2, Rheological Data) and shown in Figure 5. Reliable heat capacity

dx.doi.org/10.1021/je200355f |J. Chem. Eng. Data 2011, 56, 3242–3253

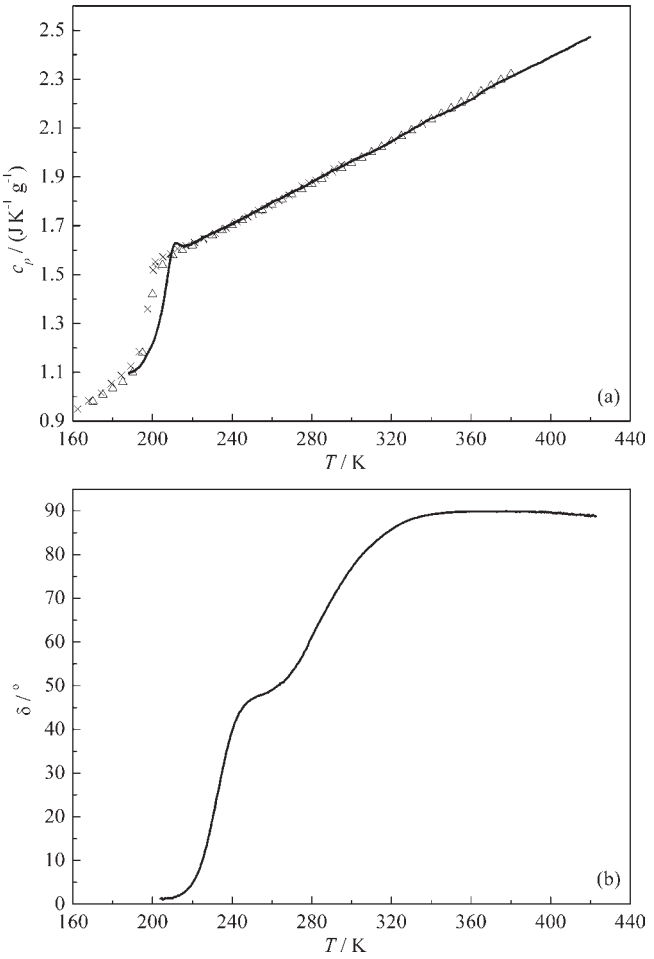

Figure 5. Heat capacity (a) and phase angle (b) for polybutene: solid line, Cannon certified viscosity standard N2700000SP; △, poly(1,1-dimethylethylene) (ref 23); ×, poly(1,1-dimethylethylene) (ref 24).

data for poly(1,1-dimethylethylene) in the amorphous state and poly(1-ethylethylene) in the crystalline and partially amorphous states are available in the literature.[22−28] The literature data for fully amorphous poly(1,1-dimethylethylene)[23,24] are included in Figure 5a. The literature values and present specific heat capacity measurements agree within the uncertainty of the methods in both the glass and liquid states.

5. DISCUSSION

The principles and experimental and computational approaches used in our prior work on the phase behavior of Maya crude oil[5] are exploited here to construct a phase diagram for Athabasca bitumen. Key and experimentally verifiable assumptions used to construct the phase diagram include:

(1) Nanofiltered samples only differ in their pentane asphaltene content. According to the SARA analysis shown in Table 1 (see refs 6 and 29 for details), the asphaltene-free composition of the maltenes is independent of the asphaltene content within the experimental error.

(2) Nanofiltered asphaltenes and maltenes are assumed to form largely separate solid and liquid phases because they are physically separable.[6] While some composition variation is expected with variation in filtration temperature,[29] it is considered of secondary importance in the present context.

(3) Athabasca maltenes and asphaltenes are assumed to be solid (crystalline and/or glass) below 190 K. No phase transitions are anticipated below this temperature. This assumption was validated previously for Maya crude oil.[21]

The independence of maltene and asphaltene phase behavior and individual phase transitions are discussed in detail below, and then the phase diagram is presented.

5.1. Independence of Nanofiltered Maltene and Asphaltene Phase Behaviors. If the apparent heat capacities of nanofiltered maltenes and asphaltenes are assumed to be independent, the heat capacities of nanofiltered samples with differing asphaltene compositions can be calculated as:

$$c_{p,\,\mathrm{sample}} = w_\mathrm{A} \cdot c_{p,\,\mathrm{A,\,app}} + (1 - w_\mathrm{A}) \cdot c_{p,\,\mathrm{M,\,app}} \qquad (3)$$

where $c_{p,\mathrm{sample}}$ is the apparent heat capacity of a sample; $c_{p,\mathrm{M,app}}$ and $c_{p,\mathrm{A,app}}$ are the apparent heat capacities of maltenes or asphaltenes, respectively; w_A is the mass fraction of asphaltenes in the sample.

This linear model was tested by fitting estimates for $c_{p,\mathrm{M,app}}$ and $c_{p,\mathrm{A,app}}$ jointly over all sets of data for five nanofiltered samples and the original bitumen at each temperature by minimizing the value of the objective function:

$$\mathrm{OF} = \frac{1}{6}\sum_{1}^{6} |c_{p,\,\mathrm{sample,\,exp}} - [w_\mathrm{A} \cdot c_{p,\,\mathrm{A,\,app}} + (1 - w_\mathrm{A}) \cdot c_{p,\,\mathrm{M,\,app}}]| \qquad (4)$$

Independence is verified if the value of the objective function is less than or equal to the experimental error of individual apparent heat capacity measurements at fixed temperature, and residuals for individual samples are also consistently less than or equal to the experimental measurement error, over the temperature range of measurements for specific samples. Deviations less than ≈0.06 J·K^{-1}·g^{-1} fall within the experimental error. Apparent heat capacity values for heating cycles 1 and 2 were fit separately. The uncertainty of the calculations of apparent heat capacities of nanofiltered maltenes is expected to be comparable to those of individual experimental heat capacity measurements and that for nanofiltered asphaltenes is estimated to be about twice the uncertainty of the experimental heat capacity measurements. The errors are larger for asphaltenes than maltenes because the most asphaltene-rich samples comprise less than 0.60 mass fraction of asphaltenes, whereas the permeates comprise as little as 0.05 mass fraction of asphaltenes.

To avoid distortion in the calculated values for nanofiltered maltenes and asphaltenes arising from the narrow low-energy first-order phase transitions occurring in the temperature range from (320 to 360) K in permeates (heating cycle 1), the small *humps* associated with this transition were replaced with "normal" heat-capacity baselines assuming fully-amorphous behavior. This avoids the appearance of a small (false) exotherm in the nanofiltered asphaltenes heat capacity profile, at 335 K, and eliminates the appearance of the first-order transition in the nanofiltered maltenes, centred at 335 K, as shown in Figure 6, which may or may not occur at that temperature. The impact of this modification is negligible even within the temperature interval (330 to 340) K where it occurs. The nature of the first-order transition is discussed in detail in Section 5.3.

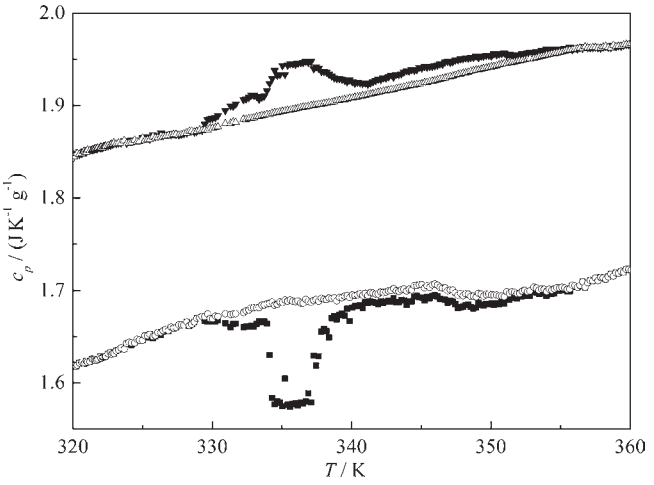

Figure 6. Apparent heat capacities for pseudocomponents calculated by eqs 3 and 4: ■, for nanofiltered asphaltenes, calculated from the original heat-capacity data; ○, for nanofiltered asphaltenes, calculated from the heat-capacity data modified in the range (320 to 360) K; ▼, for nanofiltered maltenes, calculated from the original heat-capacity data; △, for nanofiltered maltenes, calculated from the heat-capacity data modified in the range (320 to 360) K.

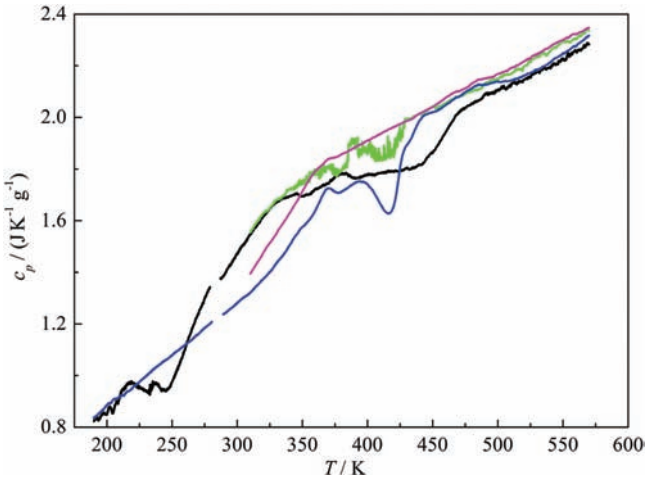

Figure 7. Apparent heat capacity of asphaltenes: computed values for nanofiltered asphaltenes—heating cycle 1 (black line) and heating cycle 2 (green line); measured values for chemically separated pentane asphaltenes—heating cycle 1 (blue line) and heating cycle 2 (pink line).

Although the phase anomaly (hump) in heating cycle 2 is also not fully reproducible, which led to larger scatter in the apparent heat capacity of asphaltenes and maltenes between (360 to 430) K, a similar replacement procedure as that for heating cycle 1 was not used since the nature of the transition is not defined, which does not provide a basis for similar interpolation.

The apparent heat capacities for nanofiltered asphaltenes and maltenes obtained from fitting the calorimetric data for the first and second heating cycles are reported in Figures 7 and 8, respectively, and the residuals are plotted in Figure 9. For both heating cycles, the average absolute value of the residuals is less than 0.02 J·g^{-1}·K^{-1}. All experimental measurements are fit within the experimental error, and nanofiltered maltenes and asphaltenes used as pseudocomponents for phase diagram

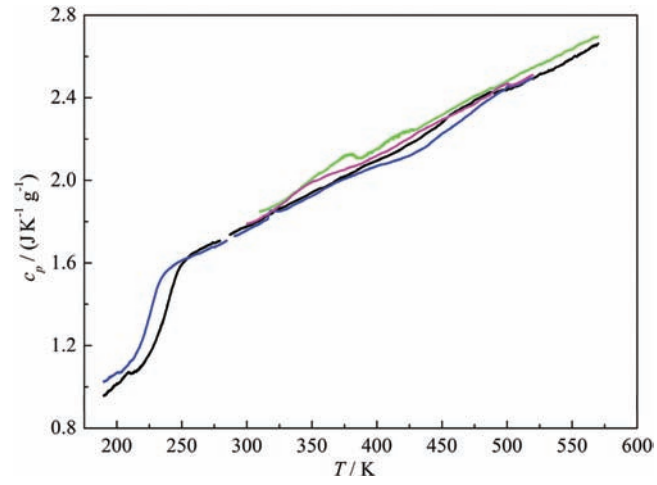

Figure 8. Apparent heat capacity of maltenes: computed values for nanofiltered maltenes—heating cycle 1 (black line) and heating cycle 2 (green line); measured values for chemically separated pentane maltenes —heating cycle 1 (blue line) and heating cycle 2 (pink line).

construction may be considered independent. This result is also consistent with our recent work indicating that nanofiltered asphaltenes from Maya crude oil and Athabasca bitumen do not associate preferentially with other SARA constituents[5,6,29] and with indirect down hole observations.[30]

A comparison of the computed values for nanofiltered maltenes and asphaltenes with the heat capacity measurements for chemically separated maltenes and asphaltenes (Figures 7 and 8) reveals noticeable differences in their phase behavior. For example, the low-temperature glass-type transition for chemically separated maltenes occurring during heating cycle 1 as well as the heat-capacity anomaly of an as-yet unrevealed nature in the temperature range (315 to 385) K during heating cycle 2 arise at lower temperatures than in nanofiltered maltenes. Their phase behaviors are otherwise similar. By contrast, the behavior of chemically separated C_5 asphaltenes differs markedly from that of the nanofiltered asphaltenes from (200 to 510) K. The phase transition in nanofiltered asphaltenes starts at a much lower temperature (260 K), shows a glass-type transition at 440 K, and does not possess an exotherm. These differences are addressed in more detail in the following sections.

5.2. Low-Temperature Glass Transition in Maltenes. Phase angle and calorimetric measurements provide information concerning phase transitions and are complementary. Phase angle approaches 0° for solid continuous samples (elastic state) and approaches 90° for liquid continuous samples (viscous state). For naphthalene + biphenyl binary mixtures, where crystalline solids are formed,[5] the end of the low-temperature plateau (phase angle = 0°), the temperature corresponding to phase angle of 45°, and the beginning of the high temperature plateau (phase angle = 90°), corresponded to 0.65, 0.50, and 0.35 volume fractions of solids, respectively. For polybutene, a glass-forming material, the calorimetric data (Figure 5a) indicate the onset of a glass transition at 201 K (with $\Delta_g c_p = 0.42$ J·K^{-1}·g^{-1}), and there is no evidence of a melting transition up to 420 K (well above the temperature evaluated as a melting point from the "two-third rule"[31,32]); thus, the polybutene sample is in a pure amorphous state. The phase angle values for polybutene start to deviate from the low-temperature plateau at about 220 K (Figure 5b), which corresponds to the end of the glass transition from the

dx.doi.org/10.1021/je200355f |J. Chem. Eng. Data 2011, 56, 3242–3253

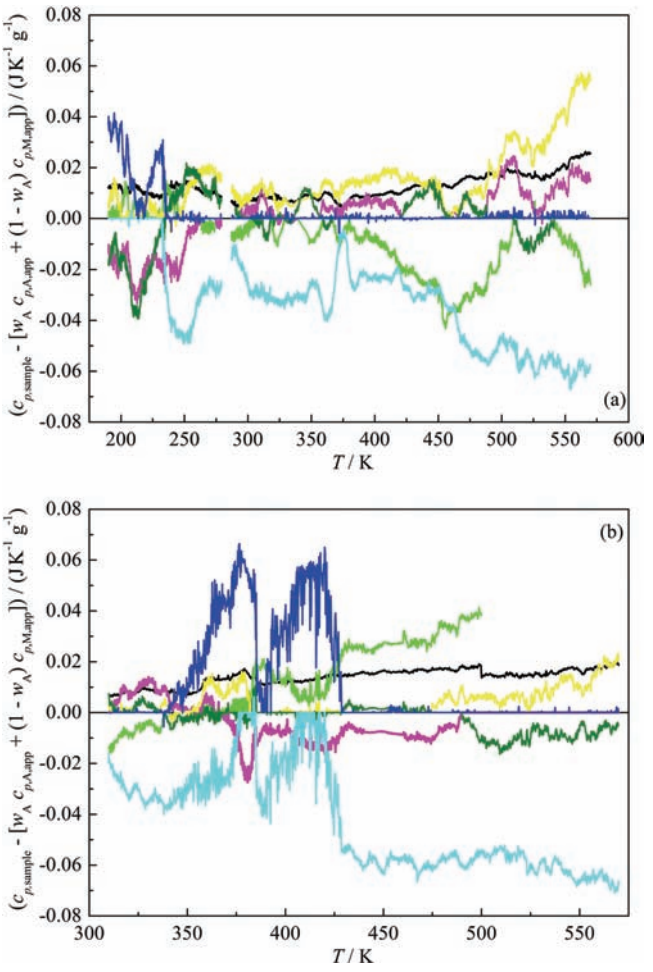

Figure 9. Residuals of the fit using eqs 3 and 4: (a) heating cycle 1, (b) heating cycle 2; black line, objective function given by eq 4; light green line, P10 with $w_A = 0.053$; pink line, P20 with $w_A = 0.104$; yellow line, P50 with $w_A = 0.136$; dark green line, AB bitumen with $w_A = 0.186$; cyan line, R200 with $w_A = 0.50$; blue line, R10 with $w_A = 0.57$.

calorimetric data. At higher temperatures, polybutene relaxes from a solid-like to a liquid-like behavior in two steps with the formation of a gel.

This apparent discrepancy in T_g values determined from calorimetric and phase angle data arises from the difference in time scales of the two measurements. During DSC experiments, a glass transition is observed when the relaxation time in a sample reaches about 200 s (for a scanning rate of 0.167 K·s^{-1}).[33,34] This is much slower than the average relaxation time (about 0.2 s) arising in the phase angle measurements at an oscillatory frequency of 1 Hz. Since the relaxation time drops by 2 to 2.5 orders of magnitude within a glass transition range detected in calorimetric measurements,[33] the T_g values from the rheological measurements correspond approximately to the end of the glass-transition observed from the calorimetric measurements.

At low temperatures, the heat capacity curves for Athabasca nanofiltered and chemically separated pentane maltenes, in Figure 8, have shapes, transformation temperature ranges, and heat capacity jumps, in Table 2, which are similar to those observed for the glass transition in polybutene (Figure 5a) and indicate the relaxation nature of the transition in maltenes. The calorimetric glass-transition ranges (Table 2) determined experimentally and calculated from the apparent heat capacities of pseudocomponents by eq 3 for maltene-rich nanofiltered samples, where the impact of asphaltenes on heat capacity values and shape is small, are also in excellent agreement. The heat capacity profile for the retentates (Figure 1) reveals the superposition of phase transitions in maltenes and asphaltenes resulting in a broad phase transformation region.

The phase angle data, Figure 4 and Table 3, cannot be compared directly with the calorimetric data for maltenes because of: (1) differing maltene/asphaltene mass ratios, (2) the overlap between asphaltene and maltene phase transitions, and (3) the significant differences in the fraction of species reaching the relaxation time equal to 0.2 s at fixed temperature in different samples. For example, the R10 sample, comprising only 0.43 mass fraction of maltenes, must be heated to much higher temperatures than maltenes to reach the same fraction with a specific relaxation time that leads to an observable rise of phase angle above the low-temperature plateau. Nevertheless, the same qualitative tendency is observed. Calorimetrically determined T_g values, Table 2, are lower than those from the rheological measurements (Table 3) due to difference in time scale of the measurements.

The frequency and temperature dependence of phase angles for Athabasca bitumen was studied previously in our laboratory.[35] The phase angle of Athabasca bitumen deviated from the low-temperature plateau at 255 K at an oscillatory frequency of 0.1 Hz, at 261 K at 1 Hz, and at 269 K at 10 Hz. All of these temperatures are greater than the T_g value of the nanofiltered maltene glass transition obtained from the DSC measurements (Table 2) and are in good agreement with the relaxation nature of a glass transformation; the smaller the time scale of measurements, the higher the measured T_g value. Additional proof for the relaxation nature of the low-temperature transition in Athabasca maltenes is the dependence of apparent heat capacity on cooling rate, that is, the appearance of a maximum in heat capacity when a sample is rapidly heated after slow cooling (Figure 3). This phenomenon is common for glasses in the glass-transition region and is due to the relaxation to lower enthalpy at slow cooling followed by a delay in structural recovery with subsequent rapid heating.[36−40] By contrast, phase-angle values for Maya crude oil, reported previously,[35] are almost independent of oscillation frequency in the comparable transition region. Maya maltenes undergo a broad first-order phase transition (melting)[5] and not a glass transition.

5.3. Partial Melting of Maltenes during the First Heating Cycle and the Enthalpy of Fusion of Maltenes. The second phase transition (first-order type) in Athabasca bitumen permeates and chemically separated C_5 maltenes in the range (310 to 360) K is considered in this section (Figure 10). The anomalies in Athabasca C_5 asphaltenes, AB R200 and AB R10 from (360 to 390) K are excluded from consideration since they tentatively belong to a broader phase transition in asphaltenes and, hence, have a different nature. The temperature ranges, the peak temperatures (referred to as transition temperatures), and the enthalpy of the transition obtained by integration of excess heat capacity are given in Table 4. There is no obvious dependence of the position and shape of the peak on the asphaltene content, but it lies at lower temperature for chemically separated C_5 maltenes in comparison to nanofiltered samples.

According to the well-known empirical "two-third rule",[31,32] the fusion and glass-transition temperatures are related as $T_g/T_{fus} \approx 2/3$ for pure compounds and simple organic mixtures. It is evident from our data (Table 4) that the transition temperatures

Table 2. Temperature Ranges for a Low-Temperature Glass Transition Obtained from DSC Results[a]

material	T_{onset} (T_g)/K	T_{end}/K	T_{mid}/K	$\Delta_g c_p$ / J·K^{-1}·g^{-1}
Maltenes, $w_A = 0$				
chemically separated C_5 maltenes	216	235	226	0.38
nanofiltered maltenes [b]	227	249	239	0.40
Nanofiltered Samples (Experiment)				
P10, $w_A = 0.053$	227	249	238	0.35
P20, $w_A = 0.104$	227	250	239	0.35
P50, $w_A = 0.136$	228	250	239	0.31
AB, $w_A = 0.186$	226	250	238	0.34
R200, $w_A = 0.50$	237	[c]	[c]	[c]
R10, $w_A = 0.57$	235	[c]	[c]	[c]
Nanofiltered Samples (Calculation from Apparent Heat Capacities of Asphaltenes and Maltenes, eqs 3 and 4)				
P10, $w_A = 0.053$	227	250	239	0.37
P20, $w_A = 0.104$	227	250	239	0.35
P50, $w_A = 0.136$	228	251	240	0.33
AB, $w_A = 0.186$	228	252	240	0.31
R200, $w_A = 0.50$	232	[c]	[c]	[c]
R10, $w_A = 0.57$	234	[c]	[c]	[c]

[a] Symbols: T_{onset}, T_{mid}, and T_{end} are the temperatures corresponding to the beginning, the middle, and the end of a glass transition; $\Delta_g c_p$ is the heat capacity jump at the glass transition. The uncertainties in temperatures of glass transitions and heat capacity jumps are estimated to be 1 K and 0.08 J·K^{-1}·g^{-1}, respectively. [b] Calculated, see Section 5.1. [c] Superposition of maltene glass transition and asphaltene phase transition.

Table 3. Characteristic Temperatures Determined from Phase-Angle Measurements[a]

sample	T_0/K	T_{45}/K	T_{90}/K
AB C_5 maltenes, $w_A = 0$	244	251	272
P10, $w_A = 0.053$	256	263	285
P20, $w_A = 0.104$	259	268	302
P50, $w_A = 0.136$	259	268	312
AB, $w_A = 0.186$	261	272	325
R200, $w_A = 0.50$	295	332	415
R10, $w_A = 0.57$	300	339	421
AB C_5 asphaltenes, $w_A = 1$ (run 1)	397	421	505
AB C_5 asphaltenes, $w_A = 1$ (run 2)	384	415	502

[a] Symbols: T_0, T_{45}, and T_{90} are the temperatures corresponding the end of the low-temperature plateau (phase angle = 0°), to phase angle of 45°, and the beginning of the high temperature plateau (phase angle = 90°), respectively. The uncertainty in the temperatures is estimated to be 1 K.

found for the first-order transition in the AB maltene-rich samples are in excellent agreement with the rule. This agreement indicates that the transition corresponds to fusion of a small portion of bitumen existing in a crystalline state, whereas the major part is in an amorphous/liquid state. Since the glass transition is associated with maltenes, the crystals arise within the maltene fraction as well. Moreover, this transition does not reappear during the second heating cycle (Figure 2), which shows the kinetic aspects of recrystallization from mixtures as complex as Athabasca bitumen. Small differences in the shape and position of the transition peak are related to the stochastic nature of crystallization processes, that is, random crystallization of fractions with different composition from such complex mixtures. This nature of the melting transition validates the replacement procedure applied in Section 5.1 to obtain the heat capacity of nanofiltered matenes in the fully amorphous state.

Pure organic compounds have a wide range of fusion enthalpies[41,42] from values close to 5 J·g^{-1} for compounds forming positionally or orientationally disordered crystals to as much as 250 J·g^{-1} for large *n*-alkanes. The fusion enthalpy

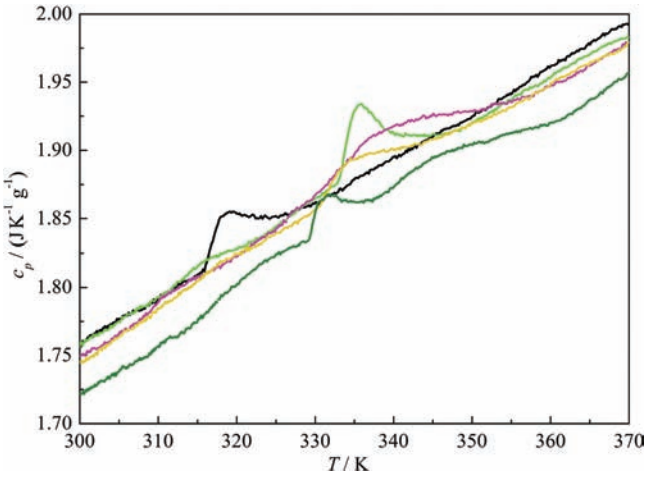

Figure 10. Temperature dependence of experimental heat capacity for Athabasca bitumen permeates in the temperature range of the first-order phase transition associated with partial melting of maltenes: black line, C_5 maltenes; light green line, P10; pink line, P20; yellow line, P50; dark green line, AB bitumen.

obtained in this work (Table 4) is below this range. So only a tiny fraction of the maltenes (less than 0.01 mass fraction) can be crystalline. The independence of phase behavior of the pseudo-components permits the estimation of the enthalpy of fusion for fully crystalline maltenes. Taking into account that enthalpy is a state function, the specific enthalpy of fusion ($\Delta_{fus}h^o$) is:

$$\Delta_{fus}h^o = \int_0^{T_{fus}} [c_{p,\,glass/liquid}(T) - c_{p,\,crystal}(T)]dT + \Delta_{cr}^{gl}h_{0K}^o \quad (5)$$

where $c_{p,glass/liquid}(T)$ and $c_{p,crystal}(T)$ are the specific heat capacities of glass (or liquid above T_g) and crystal, respectively;

dx.doi.org/10.1021/je200355f |J. Chem. Eng. Data 2011, 56, 3242–3253

Table 4. Temperature Ranges of the First-Order Phase Transitions for AB Samples from the DSC Results[a]

material	interval/K	T_{peak} (T_{trs})/K	$\Delta_{trs}h$ / J·g^{-1}	$T_{g,maltenes}/T_{trs}$
AB C_5 maltenes, $w_A = 0$	316 to 330	319	0.20	0.68[b]
P10, $w_A = 0.053$	333 to 348	336	0.29	0.68
P20, $w_A = 0.104$	324 to 358	337	0.57	0.67
P50, $w_A = 0.136$	329 to 351	335	0.25	0.68
AB, $w_A = 0.186$	329 to 337	332	0.11	0.68

[a] Symbols: T_{peak} is the temperature of the peak of the phase transition referred to as the transition temperature (T_{trs}); $T_{g,maltenes}$ is the glass transition temperature for maltenes; $\Delta_{trs}h$ is the enthalpy associated with the phase transition. The uncertainty in the temperatures is estimated to be 1 K. The relative uncertainty of $\Delta_{trs}h$ is estimated to be less than 2 %. [b] Calculated with respect to the T_g value for chemically separated C_5 maltenes; for the others the T_g value for nanofiltered maltenes is used (Table 2).

T_{fus} is the fusion temperature; $\Delta_{cr}^{gl}h_{0K}^{o}$ is the enthalpy difference between glass and crystal at $T = 0$ K.

The difference $\Delta_{cr}^{gl}h_{0K}^{o}$ is in the order of (40 to 100) J·g^{-1} depending on the molecular structure, presence of hydrogen bonding, and so forth.[43−45] Generally, it is necessary to have heat capacities for glass/supercooled liquid and crystal measured from 0 K to T_{fus} to determine this difference. As such measurements are not feasible for bitumen, values of $(\Delta_{fus}h^{o} - \Delta_{cr}^{gl}h_{0K}^{o})$ for maltenes were estimated assuming that at $T < 200$ K the heat capacities of glass and crystal are equal. Equations 1and 2 were used to approximate the crystal heat capacity. The value, $T_{fus} = 358$ K, corresponding to the end of the partial melting in P20, is the highest temperature at which crystals are detected. Thus, the integration in eq 5 was performed from (200 to 358) K. Since the low-temperature phase transition for nanofiltered asphaltenes starts within the integration range (Figure 7), the enthalpy associated with this transition was subtracted from the integral in eq 5. As samples comprise only a fraction of maltenes, the resulting expression is:

$$(\Delta_{fus}h^{o} - \Delta_{cr}^{gl}h_{0K}^{o})_{M} = (1 - w_A)^{-1} \cdot \left[\int_{200K}^{T_{fus}} (c_{p,\,sample,\,exp} - c_{p,\,sample,\,corr})\,dT - w_A \int_{200K}^{T_{fus}} (c_{p,\,A,\,app} - c_{p,\,A,\,corr})\,dT \right] \quad (6)$$

where $c_{p,sample,exp}$ and $c_{p,sample,corr}$ are the specific experimental and solid-correlation (eqs 1 and 2) heat capacities for a bitumen-related sample, respectively; T_{fus} is the temperature corresponding to the end of melting of maltenes; $c_{p,A,app}$ and $c_{p,A,corr}$ are the specific apparent (see eq 3) and solid-correlation (eqs 1−2) heat capacities for nanofiltered asphaltenes; w_A is the mass fraction of asphaltenes in a sample.

The computed enthalpy values $(\Delta_{fus}h^{o} - \Delta_{cr}^{gl}h_{0K}^{o})_{M}$ reported in Table 5 agree to within ± 4 J·g^{-1}. If the above-mentioned range for the $\Delta_{cr}^{gl}h_{0K}^{o}$ values is applied, this places the enthalpy of fusion for maltenes between (80 and 140) J·g^{-1}, which is in agreement with fusion enthalpy range (5 to 250) J·g^{-1} typical for organic compounds.[41,42]

5.4. Phase Transitions in Chemically Separated and Nanofiltered Athabasca Asphaltenes. There is a significant difference in the phase behavior of chemically and physically separated asphaltenes. During the first heating cycle, chemically separated C_5 asphaltenes undergo a broad endothermic phase transition starting at ≈310 K, ending at ≈530 K intersected by an exotherm between (391 and 430) K (Figure 7). No transition was observed at lower temperatures. The transition enthalpies were estimated to be ≈22 J·g^{-1} for the endothermic transition and ≈−4 J·g^{-1} for the exothermic one (due to arbitrary choice of a heat-capacity baseline for the exotherm, both absolute values are linearly interdependent). This behavior is similar to that of Maya C_5 asphaltenes[5] and indicates that chemically separated asphaltenes are primarily amorphous materials with only a small crystalline fraction that melts between (310 to 530) K. The presence of a crystalline fraction in chemically separated asphaltenes is consistent with a more detailed study where liquid crystalline domains were identified in pentane asphaltenes from numerous sources during the first heating cycle and the exotherm occurring during the first heating cycle was attributed to a dissolution process.[4] The continuous increase in phase angle (Figure 4) from 0° at 397 K up to the 90° plateau at 505 K does not allow us to distinguish melting from a glass transition. The phase-angle anomaly between 470 and 495 K is unlikely to be related to any specific phase transformation. There is no evidence of a specific phase transition found in the DSC measurements. It is most probably an experimental artifact when powdered asphaltenes loaded into the rheometer melt and form a continuous liquid phase.

Like the Maya C_5 asphaltenes, the phase behavior of chemically separated Athabasca C_5 asphaltenes changes drastically following the first heating−cooling cycle. During the second heating cycle, chemically separated Athabasca C_5 asphaltenes exhibit a glass transition with $T_g \approx 290$ K (extrapolation) and the heat-capacity jump of $\Delta_g c_p \approx 0.31$ J·K^{-1}·g^{-1} instead of a complex phase transition from (310 to 530) K. The absence of liquid crystal domains during the second heating cycle[4] is consistent with the formation of a completely amorphous phase (glass). This behavior shows the kinetic difficulties of recrystallization of high-molecular compounds within complex and highly viscous fluids. The observed shift in the onset temperature for the phase angle rise to lower temperatures during the second heating cycle (Table 3 and Figure 4) is also in agreement with the formation of fully amorphous state after the thermal treatment during heating cycle 1.

Nanofiltered Athabasca asphaltenes reveal a stepwise complex transformation during the first heating cycle beginning at ≈260 K (much lower than for chemically separated asphaltanes), which can be a melting and/or glass transition. A second step, a typical glass transition, has $T_g = 442$ K and $\Delta_g c_p = 17$ J·K^{-1}·g^{-1}. Similar to chemically separated asphaltenes, nanofiltered asphaltenes undergo

Table 5. Difference between the Fusion Enthalpy and Residual Zero-Point Enthalpy of Glass for Maltenes Calculated from the Athabasca Bitumen Related Sample

sample	w_A	$(\Delta_{fus}h^{o} - \Delta_{cr}^{gl}h_{0K}^{o})_{M}$ / J·g^{-1}
chemically separated C_5 maltenes	0	37
P10	0.053	36
P20	0.104	40
P50	0.136	35
AB	0.186	40
R200	0.50	33
R10	0.57	32
average value		36

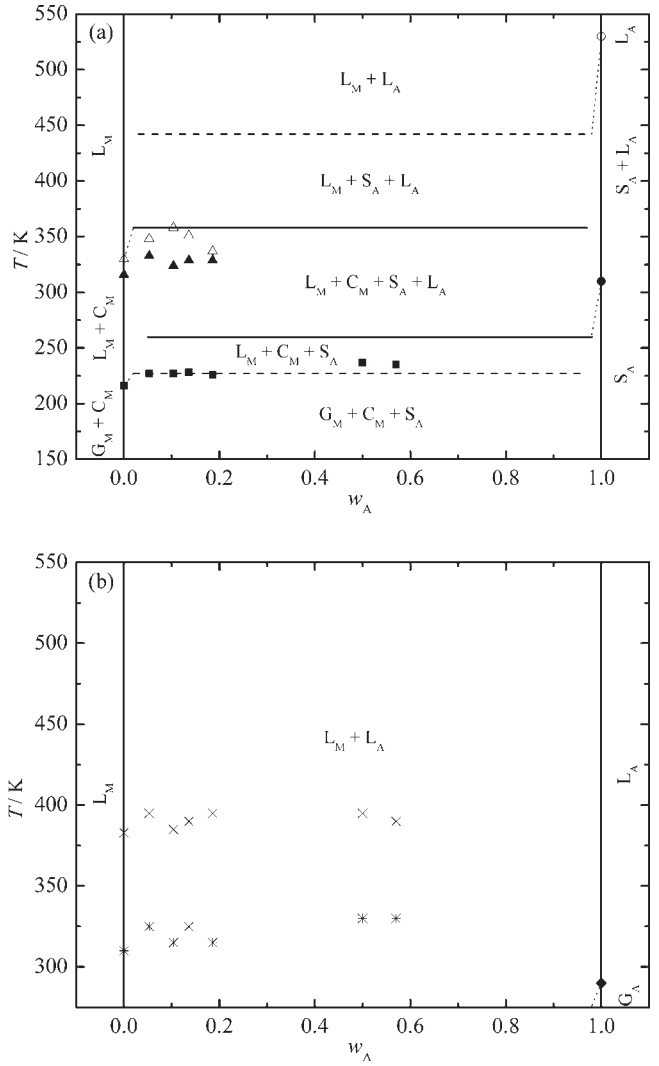

Figure 11. Phase diagram for Athabasca bitumen, heating cycle 1 (a) and heating cycle 2 (b): ■, calorimetrically defined glass transition in maltenes; ● and ○, beginning and ending of the phase transition in chemically separated asphaltenes; ▲ and △, beginning and ending of partial melting of maltenes; ∗ and ×, beginning and ending of a phase transition anomaly of an undefined nature in liquid maltenes during the second heating cycle; ◆, calorimetrically defined glass transition in chemically separated asphaltenes. Abbreviations: G_M, C_M, and L_M are glass, crystalline, and liquid maltenes, respectively; S_A, G_A, and L_A are solid (either glass or solid or both), glass, and liquid asphaltenes. Solid lines depict phases (boundaries), dashed lines reflect glass-to-liquid transitions, dotted lines link transitions in chemically separated and nanofiltered pseudocomponents.

only a broad glass transition during the second heating cycle (Figure 7). Since the apparent heat capacity of nanofiltered asphaltenes for the second heating cycle were obtained from experimental heat capacities starting 310 K and the glass transition starts well below this temperature, T_g was not determined for the second heating cycle.

5.5. Phase Diagram of Athabasca Bitumen. Pseudobinary phase diagrams for Athabasca bitumen conceived on the basis of nanofiltered asphaltenes and maltenes and reflecting the detailed analysis above are presented in Figure 11a for heating cycle 1 and in Figure 11b for heating cycle 2. Some of the transitions identified in this work are both subtle and difficult to measure. Consequently all phase boundaries should be viewed as tentative. The impact of thermal history on phase behavior is apparent. The behaviors of chemically separated maltenes and asphaltenes are also included in the diagrams for reference. Their phase behaviors differ markedly from the behaviors of corresponding species in the natural resource. Glass-to-liquid transitions are denoted as dashed lines in the diagrams; no change in the number or state of phases is implied there. Glass transitions reflect a gradual change in the relaxation time with temperature, so the dashed lines reflect the conventional definition of glass-transition temperatures.[33] Such transitions remain important though as they impact transport properties[35] and impose extrapolation limits for empirical property correlations. These latter points are important from the perspective of process development and optimization where fluid viscosity, interfaces, and diffusion play key roles. The phase behavior of Athabasca bitumen also appears to be more complex than in the case of Maya crude oil,[5] with overlapping phase transformations in maltenes and asphaltenes and the coexistence of four phases at ambient and reservoir temperatures.

If we focus on compositions around 0.20 mass fractions of asphaltenes, corresponding to the resource composition, Athabasca bitumen comprises a minimum of three phases up to ≈260 K, four phases from ≈(260 K to 360) K, three phases from (360 to 450) K, and two phases above 450 K during the first heating cycle. From an industrial perspective, mining and bitumen/sand separation processes, which occur within the (260 to 360) K temperature range, appear to operate in the four-phase region. This is the most complicated part of the phase diagram (Figure 11a), where small changes in operating conditions may have significant impacts on process outcomes. By contrast, steam-assisted gravity drainage (SAGD) and related reservoir based production processes operate at over 500 K, and typically, the temperature of subsequent surface operations does not drop below ≈370 K. Consequently such processes are governed by the simpler though less well-defined phase diagram, shown in Figure 11b, where Athabasca bitumen appears to exhibit only two phases.

6. CONCLUSIONS

A combination of rheological and calorimetric measurements performed with nanofiltered Athabasca bitumen samples showed that the phase behavior of this hydrocarbon resource is complex including several types of phase transformations (glass transition, melting, dissolution, etc.), and it is thermally irreversible within the time scale of the measurements. The phase behaviors of nanofiltered maltenes and asphaltenes in the bitumen were found to be independent. The bitumen comprises two or more phases over the temperature range up to 570 K; the phase transitions in nanofiltered maltenes and asphaltenes overlap, and up to four phases coexist from (260 to 360) K. Chemically separated C_5 asphaltenes and maltenes have a different phase behavior pattern than the nanofiltered ones and consequently differing thermophysical properties at the same temperatures, although the properties of the two maltenes are more similar than the two asphaltenes. The complex and irreversible phase behavior of Athabasca bitumen constrains the applicability of traditional hydrocarbon speciation and thermophysical property prediction methodologies for production process design, process selection, and process optimization for this key resource. The use of properties derived from chemically separated fractions is also questioned for these applications.

■ ASSOCIATED CONTENT

Supporting Information. Heat capacity data (xlsx) file: the raw heat capacity data and the heat capacity values calculated by eqs 1 and 2 for all studied Athabasca bitumen related samples and for polybutene; 2-rheological data (xlsx) file: the phase angle, complex viscosity, and elastic and viscous modulus for all studied Athabasca bitumen related samples and for polybutene. This material is available free of charge via the Internet at http://pubs.acs.org.

■ AUTHOR INFORMATION

Corresponding Author

*E-mail: jmshaw@ualberta.ca (J.M. Shaw).

Funding Sources

The authors gratefully acknowledge financial support from the sponsors of the NSERC Industrial Research Chair in Petroleum Thermodynamics: Natural Sciences and Engineering Research Council of Canada (NSERC), Alberta Innovates, KBR Energy and Chemical, Halliburton Energy Services, Imperial Oil Resources, ConocoPhillips Canada Resources Corp., Shell Canada Ltd., Nexen Inc., Virtual Materials Group (VMG), and Total E&P Canada Ltd. One of the authors, M.F., thanks the Ministry of Education of the Czech Republic under Grant MSM 604 613 7307.

■ ACKNOWLEDGMENT

The authors express thanks to Prof. C.A. Angell (Arizona State University) for fruitful discussions related to glass transition phenomena.

■ REFERENCES

(1) *Alberta's Energy Reserves 2009 and Supply/Demand Outlook 2010−2019*; ERCB Document # ST98−2010; Energy Resources Conservation Board: Calgary, Canada, 2010.

(2) Trinnaman, J.; Clarke, A., Eds. *2004 Survey of Energy Resources*, 20th ed. (World Energy Council); Elsevier: Oxford, UK, 2004.

(3) Speight, J. G. *The chemistry and technology of petroleum*, 4th ed.; CRC Press, Taylor & Francis Group: Boca Raton, FL, 2006.

(4) Bagheri, S. R.; Bazyleva, A.; Gray, M. R.; McCaffrey, W. C.; Shaw, J. M. Observation of liquid crystals in heavy petroleum fractions. *Energy Fuels* **2010**, *24*, 4327–4332.

(5) Fulem, M.; Becerra, M.; Hasan, M. D. A.; Zhao, B.; Shaw, J. M. Phase behaviour of Maya crude oil based on calorimetry and rheometry. *Fluid Phase Equilib.* **2008**, *272*, 32–41.

(6) Zhao, B.; Shaw, J. M. Composition and size distribution of coherent nanostructures in Athabasca bitumen and Maya crude oil. *Energy Fuels* **2007**, *21*, 2795–2804.

(7) Unterzaucher, J. Direct microdetermination of oxygen in organic substances. *Anal. Chem.* **1952**, *24*, 1523.

(8) Unterzaucher, J. The direct micro-determination of oxygen in organic substances. *Analyst* **1952**, *77*, 584–595.

(9) Höhne, G. W. H.; Cammenga, H. K.; Eysel, W.; Gmelin, E.; Hemminger, W. The temperature calibration of scanning calorimeters. *Thermochim. Acta* **1990**, *160*, 1–12.

(10) Cammenga, H. K.; Eysel, W.; Gmelin, E.; Hemminger, W.; Höhne, G. W. H.; Sarge, S. M. The temperature calibration of scanning calorimeters. Part 2. Calibration substances. *Thermochim. Acta* **1993**, *219*, 333–342.

(11) Sarge, S. M.; Gmelin, E.; Höhne, G. W. H.; Cammenga, H. K.; Hemminger, W.; Eysel, W. The caloric calibration of scanning calorimeters. *Thermochim. Acta* **1994**, *247*, 129–168.

(12) Gmelin, E.; Sarge, S. M. Calibration of differential scanning calorimeters. *Pure Appl. Chem.* **1995**, *67*, 1789–1800.

(13) Sarge, S. M.; Hemminger, W.; Gmelin, E.; Höhne, G. W. H.; Cammenga, H. K.; Eysel, W. Metrologically based procedures for the temperature, heat and heat flow rate calibration of DSC. *J. Therm. Anal.* **1997**, *49*, 1125–1134.

(14) Sabbah, R.; Xu-wu, A.; Chickos, J. S.; Planas Leitão, M. L.; Roux, M. V.; Torres, L. A. Reference materials for calorimetry and differential thermal analysis. *Thermochim. Acta* **1999**, *331*, 93–204.

(15) Messerly, J. F.; Guthrie, G. B.; Todd, S. S.; Finke, H. L. Low-temperature thermal data for *n*-pentane, *n*-heptadecane, and *n*-octadecane. Revised thermodynamic functions for the *n*-alkanes, C_5-C_{18}. *J. Chem. Eng. Data* **1967**, *12*, 338–346.

(16) Finke, H. L.; Gross, M. E.; Waddington, G.; Huffman, H. M. Low-temperature thermal data for the nine normal paraffin hydrocarbons from octane to hexadecane. *J. Am. Chem. Soc.* **1954**, *76*, 333–341.

(17) Chirico, R. D.; Knipmeyer, S. E.; Steele, W. V. Heat capacities, enthalpy increments, and derived thermodynamic functions for naphthalene between the temperatures 5 K and 440 K. *J. Chem. Thermodyn.* **2002**, *34*, 1873–1884.

(18) Höhne, G. W. H.; Hemminger, W. F.; Flammersheim, H.-J. *Differential Scanning Calorimetry*, 2nd ed.; Springer Verlag: Berlin, 2003.

(19) Laštovka, V.; Shaw, J. M. Predictive correlation for C_p of organic solids based on elemental composition. *J. Chem. Eng. Data* **2007**, *52*, 1160–1164.

(20) Laštovka, V.; Sallamie, N.; Shaw, J. M. A similarity variable for estimating the heat capacity of solid organic compounds: Part I. Fundamentals. *Fluid Phase Equilib.* **2008**, *268*, 51–60.

(21) Laštovka, V.; Fulem, M.; Becerra, M.; Shaw, J. M. A similarity variable for estimating the heat capacity of solid organic compounds: Part II. Application: Heat capacity calculation for ill-defined organic solids. *Fluid Phase Equilib.* **2008**, *268*, 134–141.

(22) Gaur, U.; Wunderlich, B. B.; Wunderlich, B. Heat capacity and other thermodynamic properties of linear macromolecules. VII. Other Carbon Backbone Polymers. *J. Phys. Chem. Ref. Data* **1983**, *12* (1), 29–63.

(23) Furukawa, G. T.; Reilly, M. L. Heat capacity of polyisobutylene from 0 to 380 K. *J. Res. Natl. Bur. Stand.* **1956**, *56* (5), 285–288.

(24) Ferry, J. D.; Parks, G. S. Studies on glass. XIII. Glass formation by a hydrocarbon polymer. *J. Chem. Phys.* **1936**, *4*, 70–75.

(25) Dainton, F. S.; Evans, D. M.; Hoare, F. E.; Melia, T. P. Thermodynamic functions of linear high polymers. Part IV. Stereospecific poly-α-olefines. *Polymer* **1962**, *3*, 286–296.

(26) Wilski, H.; Grewer, T. The specific heat of poly-1-butene. *J. Polym. Sci., Part C* **1964**, *6* (1), 33–41.

(27) Bares, V.; Wunderlich, B. Heat capacity of molten polymers. *J. Polym. Sci., Part B: Polymer Phys.* **1973**, *11*, 861–873.

(28) Lebedev, B. V.; Tsvetkova, L. Y.; Smirnova, N. N. Calorimetric study of thermodynamics of production of polybutene-1, polypentene-1, 4-methylpentene-1 and properties of reagents between 0 and 670 K. *J. Therm. Anal.* **1994**, *41*, 1371–1377.

(29) Zhao, B.; Becerra, M.; Shaw, J. M. On Asphaltene and Resin Association in Athabasca Bitumen and Maya Crude Oil. *Energy Fuels* **2009**, *23*, 4431–4437.

(30) Mullins, O. C.; Betancourt, S. S.; Cribbs, M. E.; Dubost, F. X.; Creek, J. L.; Andrews, A. B.; Venkataramanan, L. The colloidal structure of crude oil and the structure of oil reservoirs. *Energy Fuels* **2007**, *21*, 2785–2794.

(31) Elliot, S. R. *Physics of Amorphous Materials*, 2nd ed.; Longman Scientific and Technical: London, 1990.

(32) Johnson, W. L. Bulk Glass-Forming Metallic Alloys: Science and Technology. *MRS Bull.* **1999**, *24* (10), 42–56.

(33) Angell, C. A. Glass transition. In: *Encyclopedia of materials: Science and technology*, Vol. 4; Buschow, K. H. J., Cahn, R. W., Flemings, M. C., Ilschner, B., Kramer, E. J., Mahajan, S., Eds.; Elsevier: New York, 2001; pp 3565−3575.

(34) Angell, C. A. Structural instability and relaxation in liquid and glassy phases near the fragile liquid limit. *J. Non-Cryst. Solids* **1988**, *102*, 205–221.

(35) Bazyleva, A. B.; Hasan, M. A.; Fulem, M.; Becerra, M.; Shaw, J. M. Bitumen and heavy oil rheological properties: reconciliation with viscosity measurements. *J. Chem. Eng. Data* **2010**, *55* (3), 1389–1397.

(36) Angell, C. A.; Ngai, K. L.; McKenna, G. B.; McMillan, P. F.; Martin, S. W. Relaxation in glass forming liquids and amorphous solids. *J. Appl. Phys.* **2000**, *88* (6), 3113–3157.

(37) Wolpert, S. M.; Weitz, A.; Wunderlich, B. Time-dependent heat capacity in the glass transition region. *J. Polym. Sci., Part A* **1971**, *9* (10), 1887–1905.

(38) Crichton, S. N.; Moynihan, C. T. Structural relaxation of lead silicate glass. *J. Non-Cryst. Solids* **1988**, *102*, 222–227.

(39) Flynn, J. H. Thermodynamic properties from differential scanning calorimetry by calorimetric methods. *Thermochim. Acta* **1974**, *8*, 69–81.

(40) Moynihan, C. T.; Easteal, A. J.; Debolt, M. A.; Tucker, J. Dependence of the fictive temperature of glass on cooling rate. *J. Am. Ceram. Soc.* **1976**, *59* (1-2), 12–16.

(41) Domalski, E. S.; Hearing, E. D. Heat capacities and entropies of organic compounds in the condensed state. Volume III. *J. Phys. Chem. Ref. Data* **1996**, *25*, 1–525.

(42) Linstrom, P. J.; Mallard, W. G., Eds. *NIST Chemistry WebBook*, NIST Standard Reference Database Number 69; National Institute of Standards and Technology: Gaithersburg, MD; http://webbook.nist.gov (retrieved October 20, 2010).

(43) Kozyro, A. A.; Blokhin, A. V.; Kabo, G. J.; Paulechka, Y. V. Thermodynamic properties of some cyclohexyl esters in the condensed state. *J. Chem. Thermodyn.* **2001**, *33*, 305–331.

(44) Blokhin, A. V.; Paulechka, Y. V.; Kabo, G. J.; Kozyro, A. A. Thermodynamic properties of methyl esters of benzoic and toluic acids in the condensed state. *J. Chem. Thermodyn.* **2002**, *34*, 29–55.

(45) Kabo, G. J.; Blokhin, A. V.; Kozyro, A. A.; Diky, V. V. Heat capacities and enthalpies of transitions of 1-methylcyclopentanol and 1-chloro-l-methylcyclopentane in the condensed state. *Thermochim. Acta* **1996**, *290*, 13–30.